

PSO-based Model Identification of a Full-Scale CVT Drivetrain

Katsutoshi Yoshida and Hideki Takamatsu

Abstract—Torque transfer characteristics of the drivetrain of a production continuously variable transmission (CVT) vehicle is identified based on a particle swarm optimization (PSO) technique. The torque transfer characteristics from the CVT input shaft to the driveshaft is described by a simple nonlinear model: a single degree-of-freedom vibration model with a clearance. Based on the full-scale experimental data, the model parameters are identified by a data correction method and PSO. The simulated driveshaft torque shows good agreement with the measured torque from the experiment.

I. INTRODUCTION

Clearance-induced torsional shocks and vibrations in drivetrains are of critical concern to vehicle manufacturers [1–4]. Such torsional motions in drivetrains sometimes reduce driving stabilities and are transmitted to passengers as undesirable vibrations such as low-frequency fore-aft vibrations [5–8].

On the drivetrain vibrations, extensive studies have been reported based on several degree-of-freedom (DOF) mechanical models. The models with frictions were developed to examine the clutch engagement problems in a continuously variable transmission (CVT) vehicle [9] and a dual clutch transmission vehicle [10]. Moreover, the influence of clearance with friction was also taken into account in order to analyze transient responses of drivetrains such as the clearance-induced impulsive responses [11–13], the suppression of undesired vibrations with a nonlinear clutch damper [14], and the effect of clutch engagement on fore-aft and vertical vibrations of the vehicle body [5]. In these studies, identification of system parameters was not carried out so that some parameters were empirically estimated. For example, the parameters such as inertia and stiffness of a drivetrain can be estimated from detail drawings and measurements of the components in many cases; however, friction and damping are sometimes hardly obtainable in such manners [12].

For more accurate modeling of experimental torsional behavior, there are some attempts to identify the torsional parameters from measured data sets by using frequency domain identification, for example, on the 2-DOF engine model [15] and the 7-DOF powertrain model [16,17]. Moreover, time domain identification was carried out on the 5-DOF torsional model of turbine-generator sets [18]. In these studies, time responses of the models were in good agreement with those of the experimental data. However, they employed linear

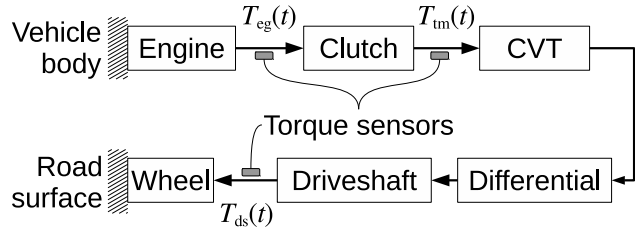


Fig. 1. Experimental measurements of the drivetrain.

models that can not describe nonlinear behavior of interest such as the clearance-induced responses in the drivetrains.

In this paper, we propose an accurate and simple nonlinear model of the clearance-induced transient torsional response of an automotive drivetrain system based on the physical data sets measured from a full-scale driving experiment on a production CVT vehicle. As the number of sensors are limited in this experiment, we restrict ourselves to two physical measurements: the transmission input torque T_{tm} and the driveshaft output torque T_{ds} , assuming that no other physical measurements of the vehicle are available for the identification purpose. Then, we develop the fewest DOF model of the torsional response of interest in view of future use in the electronic control unit (ECU).

This paper is outlined as follows. First, we examine an experimental time series of T_{ds} to derive a single DOF vibration model comprising an inertia with a viscoelastic support having a deadband. Next, we formulate a parameter identification problem that minimizes deviation between the experimental and the simulated torques. We solve the identification problem by a particle swarm optimization (PSO) method. The simulated T_{ds} by the identified model shows good agreement with the experimental T_{ds} .

II. EXPERIMENTAL DATA

The experimental vehicle is a production CVT vehicle with 1500 cc DOHC gasoline engine whose drivetrain is schematically shown in Fig. 1. The measured variables are obtained as a three-dimensional time series:

$$\mathbf{x}(t) := \left(T_{eg}(t), T_{tm}(t), T_{ds}(t) \right), \quad (1)$$

where $T_{eg}(t)$, $T_{tm}(t)$, and $T_{ds}(t)$ are the engine output shaft torque, the CVT input shaft torque, and the driveshaft output torque, respectively. The sampling rate is 1 kHz for each component of the time series.

The experiment was conducted as follows. The vehicle run along a straight horizontal track throughout the experiment. During the initial state, the vehicle was running at the

K. Yoshida is with the Department of Mechanical and Intelligent Engineering, Utsunomiya University, Yoto 7-1-2, Utsunomiya, Tochigi 321-8585, Japan yoshidak@katzlab.jp

H. Takamatsu is with Toyota Motor Corporation, 1 Toyota-Cho, Toyota, Aichi 471-8571, Japan

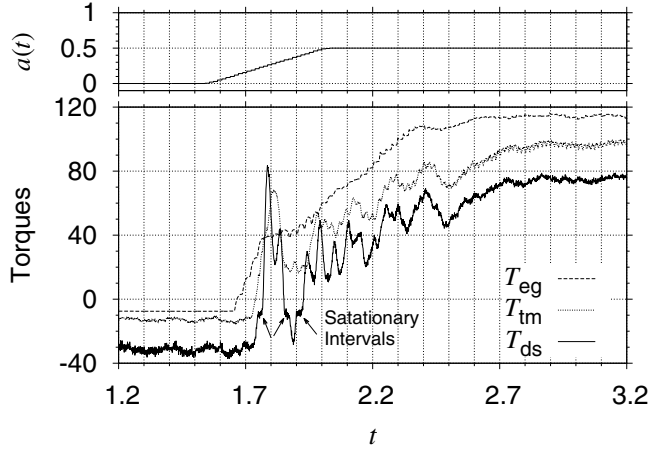


Fig. 2. A sample of experimental data as functions of time.

constant speed of 40 km/h with the throttle opening ratio $a = 0$ where a takes zero when the throttle closing while it takes unity when the throttle fully opening ($0 \leq a \leq 1$). Then, the throttle opening ratio a automatically ramped up by an experimental throttle controller from 0 to 0.5 in 0.5 seconds and maintained the constant value $a = 0.5$ thereafter. Note that during the experiment, the CVT gear ratio was temporally being varied by an ECU of the vehicle although we regard it as an unknown quantity in this paper.

Figure 2 shows a sample set of the experimental data. Note that although only $T_{tm}(t)$ and $T_{ds}(t)$ are of interest for our identification purpose in this paper, the other measured variables $a(t)$ and $T_{eg}(t)$ are also presented for reference.

All the variables in Fig. 2 are plotted as functions of time. The top graph shows the throttle opening ratio $a(t)$. The ramped increment of $a(t)$ from 0 begins at $t = 1.540$ and finished at $t = 2.033$ actually in this sample. The bottom graph shows the measured torques: $T_{eg}(t)$ from the engine output shaft, $T_{tm}(t)$ from the CVT input shaft, and $T_{ds}(t)$ from the driveshaft.

We can see from Fig. 2 that during the initial period of vibration, about $1.7 < t < 2$, $T_{ds}(t)$ has stationary intervals near $t = 1.76$, 1.86 , and 1.91 indicated by small arrows and exhibits a vibration in large amplitude that alternates negative and positive peaks. It is known that this kind of large amplitude driveshaft vibration can induce vehicle body vibrations because the driveshaft torque is directly transformed to the driving force on the vehicle body. Actually, in this experiment, the test driver in that period received large fore-aft shocks from the vehicle body, which has already been recognized as an undesirable vehicle vibration by the manufacturers [1–4].

III. DRIVETRAIN MODEL

A. Motion Model

First, we introduce a 3-DOF torsional model of the drivetrain as shown in Fig. 3. The model comprises three rotors R_0 , R_1 , and R_2 , having the inertia moments I_0 , I_1 , and I_2 , where q_0 , q_1 , and q_2 denote their angular displacements,

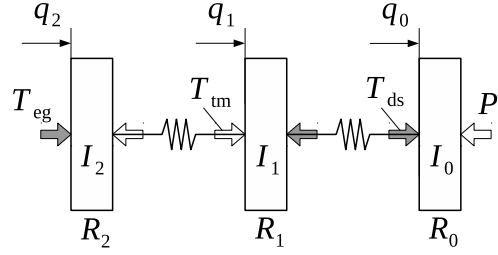


Fig. 3. 3-DOF model of the drivetrain motion.

respectively. Physically speaking, q_0 , q_1 , and q_2 represent angular displacements of the driven wheel, the CVT input shaft, and the engine output shaft, respectively. The inertia moment I_0 represents the equivalent total inertia of the vehicle body including the wheels, I_1 represents that between the CVT input shaft and the driveshaft, and I_2 represents that between the engine output shaft and the clutch input shaft.

In this model, the rotor R_2 receives a given engine torque T_{eg} and the reaction torque $-T_{tm}$ from the CVT input shaft. The rotor R_1 receives the CVT input shaft torque T_{tm} and the reaction torque $-T_{ds}$ from the driveshaft. The rotor R_0 receives the driveshaft output torque T_{ds} and the resistance torque P from the environment including running resistance, aerodynamic resistance, and so on. Therefore, the equations of motion (EOM) of this model are given by

$$\begin{cases} I_0 \ddot{q}_0 = T_{ds} - P, \\ I_1 \ddot{q}_1 = T_{tm} - T_{ds}, \\ I_2 \ddot{q}_2 = T_{eg} - T_{tm}. \end{cases} \quad (2)$$

Introducing the relative angular displacements:

$$\theta := q_1 - q_0, \quad \psi := q_2 - q_1, \quad (3)$$

we have a relative expression of (2) as

$$\begin{cases} \ddot{q}_0 = \frac{1}{I_0}(T_{ds} - P), \\ \ddot{\theta} = -\frac{1}{I_0}(T_{ds} - P) + \frac{1}{I_1}(T_{tm} - T_{ds}), \\ \ddot{\psi} = \frac{1}{I_1}T_{ds} - \left(\frac{1}{I_2} + \frac{1}{I_1}\right)T_{tm} + \frac{1}{I_2}T_{eg}. \end{cases} \quad (4)$$

B. Vibration Model

To focus on the vibrating term in the EOM (4), it is reasonable to assume that I_0 is sufficiently large because I_0 mostly represents the total vehicle body inertia. Thus, we take the limit $I_0 \rightarrow \infty$ in (4). In this limit, the first equation in (4) is reduced into $\ddot{q}_0 = 0$ that implies the algebraic relation $P = T_{ds}$. Meanwhile, the second and third equations are reduced into the following form:

$$\begin{cases} \ddot{\theta} = \rho_1(T_{tm} - T_{ds}), \\ \ddot{\psi} = \rho_1 T_{ds} - (\rho_1 + \rho_2)T_{tm} + \rho_2 T_{eg}, \quad \rho_i := (I_i)^{-1}. \end{cases} \quad (5)$$

These describe vibrations of the relative angles θ and ψ , independent of q_0 . Therefore, we have obtained the 2-DOF model (5) of the torsional vibration of the drivetrain, whose mechanical description can be given in Fig. 4.

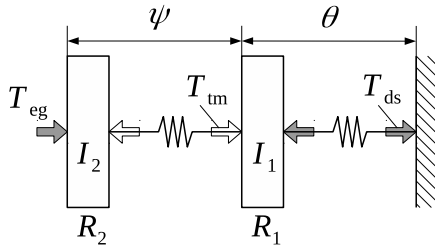


Fig. 4. 2-DOF model of the drivetrain vibration.

C. Modeling of Torque Transfer Characteristics

As we focus on the torque transfer characteristics from T_{tm} to T_{ds} , we develop a closed-form expression of T_{ds} as a function of θ and $\dot{\theta}$ of the following form:

$$T_{ds} = F(\theta, \dot{\theta}). \quad (6)$$

To specify $F(\theta, \dot{\theta})$, we suppose that the stationary intervals in Fig. 2 are induced by a total backlash of gears and couplings between the rotor R_1 and the fixed base, or, by a clearance type nonlinearity with respect to θ . We also suppose that this clearance induces torsional impact behavior of the rotor R_1 . Such torque transfer characteristics can be modeled simply by an impact model of the following form:

$$T_{ds} = F(\theta, \dot{\theta}) = \begin{cases} k^-(\theta + \mu) + c^-\dot{\theta} & (\theta < -\mu), \\ 0 & (|\theta| \leq \mu), \\ k^+(\theta - \mu) + c^+\dot{\theta} & (\theta > \mu), \end{cases} \quad (7)$$

where μ is a width of the clearance, c^- and k^- are viscoelastic coefficients during the backward contact between the gear teeth, and c^+ and k^+ are those during the forward contact. In general, smoothing functions [14,19] are often applied to build accurate impact models. We also consider a smoothed version of the impact model (7) as

$$T_{ds} = F_\sigma(\theta, \dot{\theta}) := G_\sigma(\theta, \mu, k^-, k^+) + H_\sigma(\theta, \mu, c^-, c^+)\dot{\theta}, \quad (8)$$

with the smoothed functions:

$$G_\sigma(\theta, \mu, k^-, k^+) := -k^-\phi_1(-\theta - \mu; \sigma) + k^+\phi_1(\theta - \mu; \sigma), \quad (9)$$

$$H_\sigma(\theta, \mu, c^-, c^+) := c^-\phi_2(-\theta - \mu; \sigma) + c^+\phi_2(\theta - \mu; \sigma), \quad (10)$$

where $\phi_1(\cdot; \cdot)$ and $\phi_2(\cdot; \cdot)$ are a smoothed unit ramp function and a smoothed unit step function, respectively, given by

$$\phi_1(x; \sigma) := \frac{1 + \tanh(\sigma x)}{2}, \quad \phi_2(x; \sigma) := \frac{\ln\{1 + \exp(\sigma x)\}}{\sigma}, \quad (11)$$

where σ represents steepness of these functions. As σ increases, the smoothed impact model $F_\sigma(\theta, \dot{\theta})$ in (8) converges to $F(\theta, \dot{\theta})$ in (7). For example, Fig. 5 shows $G_\sigma(\theta, 0.2, 1, 2)$ and $H_\sigma(\theta, 0.2, 0.5, 1)$ for $\sigma = 40$ and 10^3 .

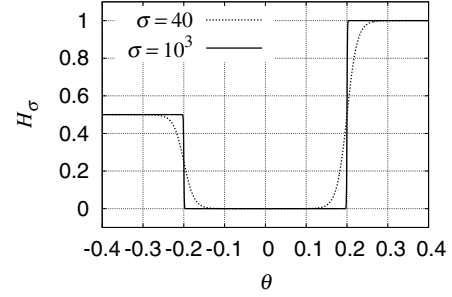
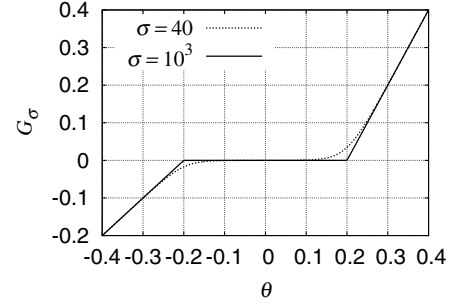


Fig. 5. Smoothing functions for $\sigma = 40$ and 10^3 .

IV. IDENTIFICATION PROBLEM

A. Data Correction Approach

In the experimental time series in Fig. 2, the stationary intervals of the driveshaft torque $T_{ds}(t)$, indicated by small arrows, take negative values $T_{ds} = \Delta_{ds} \approx -9$. We suppose that these stationary intervals of $T_{ds} = \Delta_{ds} \neq 0$ are caused by some deadband characteristics, for example, due to teeth clearances of the experimental vehicle. However, the mathematical model (8) is defined to output $T_{ds} = 0$ inside the deadband $|\theta| \leq \mu$. The difference can be corrected by shifting the model with a constant Δ_{ds} as

$$T_{ds} = F_\sigma(\theta, \dot{\theta}) + \Delta_{ds}. \quad (12)$$

In this paper, we employ an equivalent expression:

$$S_{ds} := T_{ds} - \Delta_{ds} = F_\sigma(\theta, \dot{\theta}), \quad (13)$$

where Δ_{ds} is an amplitude-shift.

The amplitude-shift Δ_{ds} in the physical vehicle can be caused by mechanical frictions in the drivetrain that is rotating in one direction. In contrast, such shift does not appear in the model (5) and (8) because the model does not produce a steady rotation; the steady rotation is approximated by a stationary state $\theta = \psi = 0$.

We also suppose that T_{tm} contains an amplitude-shift Δ_{tm} as well, and thus introduce an amplitude-shifted CVT input shaft torque as

$$S_{tm} := T_{tm} - \Delta_{tm}. \quad (14)$$

B. Problem Formulation

Suppose that a two-dimensional time series $\mathbf{y}(t) := (T_{tm}(t), T_{ds}(t))$ is measured from the experiment. Then, combining (8), (13), (14), and the second equation of (5),

we describe the dynamics from $T_{\text{im}}(t)$ to $T_{\text{ds}}(t)$ by a single DOF model in the following form:

$$\ddot{\theta} = \rho_1 \{S_{\text{im}} - F_{\sigma}(\theta, \dot{\theta})\}, \quad S_{\text{im}} := T_{\text{im}}(t) - \Delta_{\text{im}}, \quad (15a)$$

$$F_{\sigma}(\theta, \dot{\theta}) := G_{\sigma}(\theta, \mu, k^-, k^+) + H_{\sigma}(\theta, \mu, c^-, c^+) \dot{\theta}, \quad (15b)$$

$$S_{\text{ds}}^* := F_{\sigma}(\theta, \dot{\theta}), \quad T_{\text{ds}}^* := S_{\text{ds}}^* + \Delta_{\text{ds}}. \quad (15c)$$

The numerical solution $T_{\text{ds}}^*(t)$ of (15) yields the simulated driveshaft torque, which is to be compared with the measured $T_{\text{ds}}(t)$.

The single DOF model (15) has nine model parameters:

$$\mathbf{p} := (\rho_1, k^-, k^+, c^-, c^+, \mu, \sigma, \Delta_{\text{ds}}, \Delta_{\text{im}}). \quad (16)$$

To estimate \mathbf{p} from $\mathbf{y}(t)$, we solve the following optimization problem:

$$\begin{aligned} \underset{\mathbf{p}}{\text{Minimize}} E(\mathbf{p}) &:= \frac{1}{t_2 - t_1} \int_{t_1}^{t_2} |T_{\text{ds}}^*(\tau) - T_{\text{ds}}(\tau)| d\tau \\ &= \frac{1}{t_2 - t_1} \int_{t_1}^{t_2} |S_{\text{ds}}^*(\tau) - S_{\text{ds}}(\tau)| d\tau, \end{aligned} \quad (17)$$

where the cost function $E(\mathbf{p})$ evaluates absolute deviations of the simulated driveshaft torque $T_{\text{ds}}^*(t)$ inside the time interval $t_1 \leq t \leq t_2$ of interest.

In numerical calculations in Section V, the cost function $E(\mathbf{p})$ is evaluated as follows. We numerically solve the model (15) for the constant input $S_{\text{im}}(t) = S_{\text{im}}(t_1)$ to determine the initial equilibrium $\bar{\theta}(t_1)$ at $t = t_1$. Then, we obtain the numerical solution of (15) starting from

$$\theta(t_1) = \bar{\theta}(t_1), \quad \dot{\theta}(t_1) = 0 \quad (18)$$

for the variable $T_{\text{im}}(t)$. Thus, we have

$$\begin{aligned} E(\mathbf{p}) &= \frac{1}{m} \sum_{i=1}^m |F_{\sigma}(\theta(t^i), \dot{\theta}(t^i)) - S_{\text{ds}}(t^i)|, \\ t^i &:= t_1 + i\Delta t, \quad t^m := t_2, \end{aligned} \quad (19)$$

where Δt is a sampling interval of $\mathbf{T}(t)$. The Δt is also taken as the time step of the numerical solution.

To evaluate accuracy of the abovementioned modeling, we introduce an index of model quality by

$$Q(\mathbf{p}) := \left(1 - \frac{E(\mathbf{p})}{E_0}\right) \times 100, \quad (20)$$

where

$$E_0 := \frac{1}{m} \sum_{i=1}^m |S_{\text{ds}}(t^i)| \quad (21)$$

is a mean absolute amplitude of the measured $S_{\text{ds}}(t) = T_{\text{ds}}(t) - \Delta_{\text{ds}}$.

C. Particle Swarm Optimization

As the state equation (15a) contains a nonlinear function $F_{\sigma}(\theta, \dot{\theta})$, it is required to apply a nonlinear optimization technique to solve the problem in (17). We employ a particle swarm optimization (PSO) technique to achieve faster convergence than other methods. A brief overview of PSO is provided below (see the references [20,21] for details).

Consider an optimization problem in the following form:

$$\underset{\mathbf{p}}{\text{Minimize}} E(\mathbf{p}), \quad (22)$$

where $\mathbf{p} := (p_1, p_2, \dots, p_M) \in D \subset R^M$ is an M -dimensional vector and $E(\mathbf{p})$ is a real-valued cost function positive definite.

In PSO, a swarm of N candidate solutions, $\{\mathbf{p}^1, \dots, \mathbf{p}^N\}$, is called particles. The particles explore the M -dimensional domain D in search of the global solution

$$\mathbf{p}_0 = \arg \min_{\mathbf{p}} E(\mathbf{p}). \quad (23)$$

The particle positions are recursively updated by

$$\begin{cases} \mathbf{p}^i(k+1) = \mathbf{p}^i(k) + \mathbf{v}^i(k), \\ \mathbf{v}^i(k+1) = \eta_0(k)\mathbf{v}^i(k) + \eta_1(k)\{\mathbf{P}^i(k) - \mathbf{p}^i(k)\} \\ \quad + \eta_2(k)\{\mathbf{G}(k) - \mathbf{p}^i(k)\}, \end{cases} \quad (24)$$

for $k = 0, 1, \dots, k_{\text{max}}$, where $\mathbf{p}^i(k)$ is a position of i th particle at iteration k , $\mathbf{v}^i(k)$ is a corresponding velocity, and $\eta_l(k)$ ($l = 0, 1, 2$) are random numbers. $\mathbf{P}^i(k)$ is a position of i th particle taking the lowest cost among $\mathbf{p}^i(0), \dots, \mathbf{p}^i(k)$, which is called a personal best. $\mathbf{G}(k)$ is a position of the particle that has the lowest cost among all the particles for all iteration $j \leq k$, which is called a global best.

Note that in general, the term $\mathbf{v}^i(k)$ in the second equation of (24) is sometimes taken as $\mathbf{v}^i(k+1)$ although results of optimization were not sensitive to such alternation at least in our case.

Therefore, the solution \mathbf{p}_0 of the optimization in (22) is approximately obtained by

$$\mathbf{p}_0 \approx \mathbf{G}(k). \quad (25)$$

In this paper, $\eta_0(k)$, $\eta_1(k)$, and $\eta_2(k)$ are taken as uniform random numbers over the intervals $[0, w]$, $[0, p_1]$, and $[0, p_2]$, respectively. The initial search domain $D_0 \subset D$ is taken as an M -dimensional hypercuboid:

$$D_0 := [a_1, b_1] \times \dots \times [a_M, b_M]. \quad (26)$$

The initial particle positions $\mathbf{p}^i(0)$ are taken at n^M uniform grid points on D_0 . Thus, $N := n^M$ represents the number of the particles. All the initial particle velocities are set to zero.

V. IDENTIFICATION RESULT

A. Condition of Identification

The condition of identification is empirically selected as follows. The PSO parameters are set to $w = 1$, $p_1 = p_2 = 0.4$, $M = 9$, and $n = 2$. The initial search domain in (26) is taken as

$$\begin{aligned} D_0 &= [1, 2] \times [10^3, 10^4] \times [10^3, 10^4] \\ &\quad \times [10, 20] \times [10, 20] \times [10^{-3}, 5 \times 10^{-3}] \\ &\quad \times [10^3, 5 \times 10^3] \times [-10, -5] \times [10, 15]. \end{aligned} \quad (27)$$

Thus, the number of particles is $N = n^M = 512$. The time interval of $E(\mathbf{p})$ in (19) is selected as $[t_1, t_2] = [1.5, 3]$ so that it covers the initial stationary state for $t < 1.6$, the large amplitude vibration for $1.7 < t < 2.6$, and the final stationary state for $t > 2.8$ (see Fig. 2).

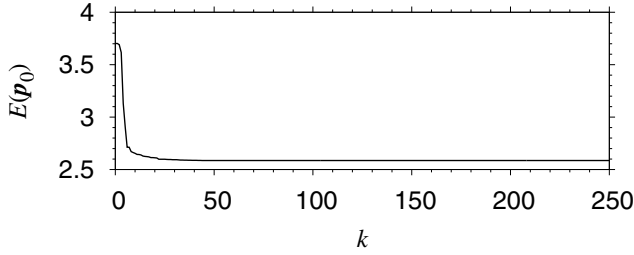


Fig. 6. The cost $E(\mathbf{p}_0)$ as a function of the PSO iteration k .

TABLE I
IDENTIFIED PARAMETER \mathbf{p}_0 AT $k = 250$.

Components	Values
ρ_1 [(kg m ²) ⁻¹]	1.42855
k_1^- [N/rad]	2.94791×10^3
k_1^+ [N/rad]	8.70064×10^3
c_1^- [Ns/rad]	4.10333
c_1^+ [Ns/rad]	1.92283×10
μ [rad]	3.55701×10^{-3}
σ	1.13281×10^3
Δ_{ds} [Nm]	-7.40521
Δ_{tm} [Nm]	1.29998×10

B. Simulated Result

Applying the method and condition in Sections IV and V-A, we identified the model parameter \mathbf{p} in (16) that simulates the experimental data $\mathbf{y}(t) = (T_{tm}(t), T_{ds}(t))$ in Fig. 2.

Figure 6 shows the cost $E(\mathbf{p}_0)$ as a function of the PSO iteration k . It is shown that the value of $E(\mathbf{p}_0)$ rapidly decreases and mostly converges after $k = 100$. The cost takes $E(\mathbf{p}_0) \approx 2.58573$ at $k = 250$ where the parameter \mathbf{p} is identified as \mathbf{p}_0 listed in Table I.

Figure 7 shows time histories of the driveshaft torques. The solid line indicates the measured $S_{ds}(t)$, already shown in Fig. 2 as $T_{ds}(t)$. The dashed line indicates the simulated $S_{ds}^*(t)$ that is a numerical solution of the model (15) with the identified \mathbf{p}_0 in Table I, subjected to the measured $S_{tm}(t)$. The simulated torque $S_{ds}^*(t)$ is mostly in good agreement with the measured $S_{ds}(t)$. The simulated $S_{ds}^*(t)$ reproduces presence of all the peaks, the ravines, and the stationary intervals, labeled by P_i , R_i , and S_i ($i = 1, 2, 3$), respectively. And it mostly reproduces the waveform. The model quality takes $Q(\mathbf{p}_0) = 94.9\%$.

The result implies that the large fore-aft vehicle body vibration observed in the experiment, due to the driveshaft vibration, can be mostly simulated by the single DOF model (15) with \mathbf{p}_0 in Table I.

However, minor disagreement in detail is also found in Fig. 7. In particular, the amplitudes are different between $S_{ds}(t)$ and $S_{ds}^*(t)$ near the peaks and ravines P1, P2, R2, and R3, and the waveform of the simulated $S_{ds}^*(t)$ is slightly delayed from that of the measured $S_{ds}(t)$. One possible explanation for this delay is different transmission delays between the experimental signals of $T_{tm}(t)$ and $T_{ds}(t)$.

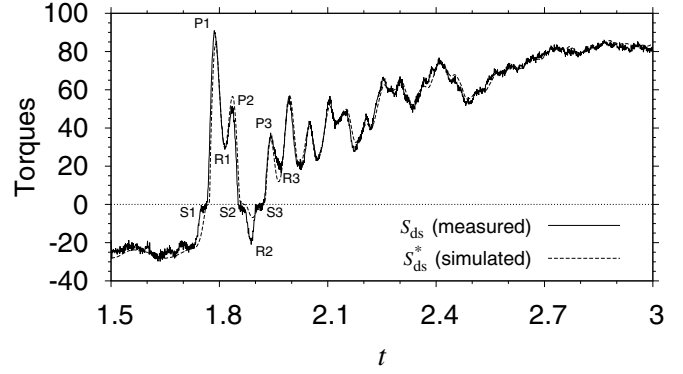


Fig. 7. Measured and simulated driveshaft torques.

VI. CONCLUSION

We conducted parameter identification of a drivetrain model of a production CVT vehicle with 1500 cc DOHC gasoline engine that exhibits large amplitude fore-aft vibrations during acceleration. First, we developed a nonlinear single DOF vibration model with clearance to describe the torque transfer characteristics from the CVT input shaft torque $T_{tm}(t)$ to the driveshaft output torque $T_{ds}(t)$. Next, we parameterized the model by a nine-dimensional parameter vector including the amplitude-shifting parameters. We employed a PSO method to solve the identification problem.

The result showed that the simulated driveshaft output torque is mostly in good agreement with the measured driveshaft output torque.

Therefore, it is concluded that the torque transfer characteristics from the CVT input torque to the driveshaft output torque in the drivetrain considered can be described by the fewest DOF vibration model with clearance.

In future work, we plan to improve accuracy of the identification, focusing on the different transmission delays among the experimental signals. We also plan to identify the overall torque transfer model from the engine output shaft torque $T_{eg}(t)$ to the driveshaft torque $T_{ds}(t)$ as a basis of developing vibration suppression control of the drivetrain.

VII. ACKNOWLEDGMENTS

We would like to thank Toyota Motor Corporation for their financial and technical support. We also appreciate the valuable feedback offered by Dr. Munehisa Sekikawa, Shigeki Matsumoto, and Shusuke Ishikawa at Utsunomiya University.

REFERENCES

- [1] S. Okabe and Y. Murayama, "Engine transient output characteristics and acceleration/deceleration shocks in FF vehicles," *Mitsubishi Motors Technical Review (in Japanese)*, vol. 2, 1989, pp. 38–45.
- [2] M. Inoue, "Analysis on acceleration/deceleration shock and vibration in FF vehicle," *Mazda Technical Review (in Japanese)*, vol. 11, 1993, pp. 84–91.
- [3] M. Yoshikawa and A. Nagamatsu, "Transient excitation torque of shock in operation for acceleration (1st report investigation of occurrence mechanism)," *Transactions of Society of Automotive Engineers of Japan (in Japanese)*, vol. 31, no. 2, 2000, pp. 35–40.

- [4] H. Moriura, "A study of vehicle acceleration shock: Analysis of driveability model and transient excitation torque rise," *Transactions of the Japan Society of Mechanical Engineers. C (in Japanese)*, vol. 69, no. 688, 2003, pp. 3228–3235.
- [5] E. M. A. Rabeih and D. A. Crolla, "Coupling of driveline and body vibrations in trucks," *SAE Conference Transactions on International Trucks and Bus Meeting and Exposition*, vol. 1203, 1996, pp. 17–26.
- [6] Y. Qiu and M. Griffin, "Transmission of foreaft vibration to a car seat using field tests and laboratory simulation," *Journal of Sound and Vibration*, vol. 264, no. 1, 2003, pp. 135–155.
- [7] N. Nawayseh and M. J. Griffin, "Tri-axial forces at the seat and backrest during whole-body fore-and-aft vibration," *Journal of Sound and Vibration*, vol. 281, no. 3-5, 2005, pp. 921–942.
- [8] M. Morioka and M. J. Griffin, "Frequency weightings for fore-and-aft vibration at the back: effect of contact location, contact area, and body posture," *Industrial health*, vol. 48, no. 5, 2010, pp. 538–549.
- [9] J. Kim, "Launching performance analysis of a continuously variable transmission vehicle with different torsional couplings," *Journal of Mechanical Design*, vol. 127, no. 2, 2005, pp. 295–301.
- [10] P. D. Walker and N. Zhang, "Modelling of dual clutch transmission equipped powertrains for shift transient simulations," *Mechanism and Machine Theory*, vol. 60, 2013, pp. 47–59.
- [11] A. Crowther and N. Zhang, "Torsional finite elements and nonlinear numerical modelling in vehicle powertrain dynamics," *Journal of Sound and Vibration*, vol. 284, no. 3-5, 2005, pp. 825–849.
- [12] A. R. Crowther, R. Singh, N. Zhang, and C. Chapman, "Impulsive response of an automatic transmission system with multiple clearances: Formulation, simulation and experiment," *Journal of Sound and Vibration*, vol. 306, no. 3-5, 2007, pp. 444–466.
- [13] A. R. Crowther, C. Janello, and R. Singh, "Quantification of clearance-induced impulsive sources in a torsional system," *Journal of Sound and Vibration*, vol. 307, no. 3-5, 2007, pp. 428–451.
- [14] L. Li and R. Singh, "Analysis of start-up transient for a powertrain system with a nonlinear clutch damper," *Mechanical Systems and Signal Processing*, 2015, pp. 1–20.
- [15] F. Östman and H. T. Toivonen, "Torsional system parameter identification of internal combustion engines under normal operation," *Mechanical Systems and Signal Processing*, vol. 25, no. 4, 2011, pp. 1146–1158.
- [16] F. Ponti, "Development of a torsional behavior powertrain model for multiple misfire detection," *Journal of Engineering for Gas Turbines and Power*, vol. 130, no. 2, 2008, pp. 022803:1–13.
- [17] F. Ponti and L. Solieri, "Analysis of the interactions between indicated and reciprocating torques for the development of a torsional behavior model of the powertrain," *Journal of Engineering for Gas Turbines and Power*, vol. 130, no. 6, 2008, pp. 062803:1–9.
- [18] M. Brown and C. Grande-Moran, "Torsional system parameter identification of turbine-generator sets," *IEEE Transactions on Energy Conversion*, vol. 12, no. 4, 1997, pp. 304–309.
- [19] T. Kim, T. Rook, and R. Singh, "Effect of smoothening functions on the frequency response of an oscillator with clearance non-linearity," *Journal of Sound and Vibration*, vol. 263, no. 3, 2003, pp. 665–678.
- [20] J. Kennedy and R. Eberhart, "Particle swarm optimization," *Proceedings of IEEE International Conference on Neural Networks*, vol. 4, 1995, pp. 1942–1948.
- [21] A. P. Engelbrecht, *Fundamentals of Computational Swarm Intelligence*. John Wiley & Sons, 2005.